# A stratigraphically controlled multiproxy chronostratigraphy for the eastern Mediterranean

J. S. L. Casford,[1] R. Abu-Zied,[2] E. J. Rohling,[3] S. Cooke,[4] C. Fontanier,[5] M. Leng,[6] A. Millard,[7] and J. Thomson[3]

Received 17 January 2007; revised 25 June 2007; accepted 19 July 2007; published 19 December 2007.

[1] An Accelerator Mass Spectrometry (AMS) $^{14}C$ dated multiparameter event stratigraphy is developed for the Aegean Sea on the basis of highly resolved (centimeter to subcentimeter) multiproxy data collected from four late glacial to Holocene sediment cores. We quantify the degree of proportionality and synchroneity of sediment accumulation in these cores and use this framework to optimize the confidence levels in regional marine, radiocarbon-based chronostratigraphies. The applicability of the framework to published, lower-resolution records from the Aegean Sea is assessed. Next this is extended into the wider eastern Mediterranean, using new and previously published high-resolution data from the northern Levantine and Adriatic cores. We determine that the magnitude of uncertainties in the intercore comparison of AMS $^{14}C$ datings based on planktonic foraminifera in the eastern Mediterranean is of the order of ±240 years (2 SE). These uncertainties are attributed to synsedimentary and postsedimentary processes that affect the materials dated. This study also offers a background age control that allows for vital refinements to radiocarbon-based chronostratigraphy in the eastern Mediterranean, with the potential for similar frameworks to be developed for any other well-studied region.

**Citation:** Casford, J. S. L., R. Abu-Zied, E. J. Rohling, S. Cooke, C. Fontanier, M. Leng, A. Millard, and J. Thomson (2007), A stratigraphically controlled multiproxy chronostratigraphy for the eastern Mediterranean, *Paleoceanography*, *22*, PA4215, doi:10.1029/2007PA001422.

## 1. Introduction and Rationale

[2] The Aegean and Mediterranean Seas are of particular importance to palaeoceanography, as the limited volumes of these basins promote rapid responses to climatic change. Because of the restricted communication with the open ocean, these responses are also amplified in comparison with oceanic signals. Together with the enhanced sediment accumulation rate common in marginal basins, this allows detailed records of change to be preserved, and facilitates high-resolution sampling [*Bethoux et al.*, 1999]. However, to interpret this wealth of information accurately, good dating constraints are essential [*Sarnthein et al.*, 2000].

[3] Unfortunately, high accumulation rates commonly increase the probability of sediment reworking. It has been suggested that much of the sediment in the Mediterranean is redeposited, with some estimates ranging as high as 75% [*Stanley*, 1985]. Another pervasive problem in marine cores is bioturbation, which mixes older and more recent material. Hence individual AMS dating results are not as reproducible as one would wish. Careful sample selection can increase the accuracy of individual datings, but even small amounts of allochthonous "old" carbon, normally impossible to detect when picking material, may cause significant anomalies, biasing results toward older ages. For example, a 10% increase in "dead" carbon in a sample will result in an age biasing of ~800 radiocarbon convention years.

[4] *Jorissen et al.* [1993] reported wide dating ranges for the timing of I/II and II/III biozonal boundaries in the Mediterranean, spanning 950 and 1270 years, respectively. The association of these boundaries with the global glacial Terminations 1a and 1b in their records suggests that the dating range is not real, but a likely artifact due to dating uncertainties. *Jorissen et al.* [1993] also note offsets in the radiocarbon ages for a number of evident lithological horizons between Adriatic cores IN68-9 and IN68-5 (only 100 km apart), with offsets nonsystematically varying between 300 and 1400 years, suggesting dating uncertainties. Moreover sequences of dating within a single core may also highlight uncertainties. For example, *Jorissen et al.* [1993] show several instances of dating "reversals" within individual cores. Similarly core KET 8216 from the Adriatic shows an 800 year difference between virtually adjacent datings from below and above the base of the sapropel (S1) [*Fontugne et al.*, 1989]. These datings are only 3 cm apart and the suggested separation would require an almost threefold reduction in the average sedimentation rate of the core. Although individual datings may be offset from "true" age by variation in the reservoir age, this is unlikely to explain substantial dating reversals or large age differ-

[1]Department of Geography, Durham University, Science Site, Durham, UK.
[2]Geology Department, Mansoura University, El-Mansoura, Egypt.
[3]National Oceanography Centre, European Way, Southampton, UK.
[4]Department of Earth and Ocean Sciences, University of Waikato, Hamilton, New Zealand.
[5]Laboratoire des Bio-Indicateurs Actuels et fossils, UFR Sciences, Angers, France.
[6]School of Geography, University of Nottingham, Nottingham, UK.
[7]Department of Archaeology, Durham University, Science Site, Durham, UK.


0883-8305/07/2007PA001422$12.00

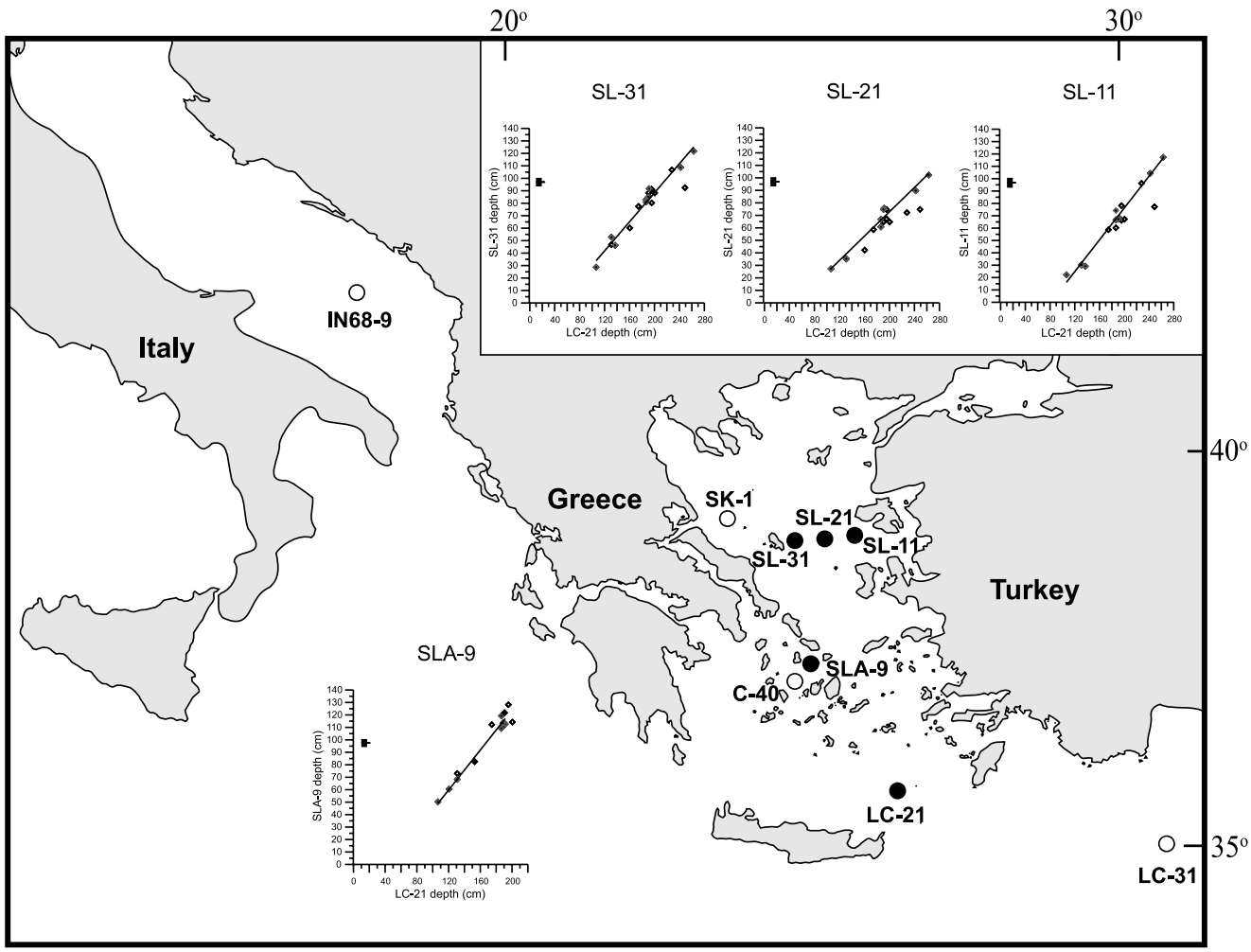


**Figure 1.** Core locations. Solid circles indicate cores presented in this study, and open circles are core sites from the published literature (see text for references). Inset graphs show regressions of the depth occurrence (in centimeters down core) for primary events (solid diamonds) and ancillary events (open diamonds) detailed in this study. A 2 SE error bar is included for the *x* axis.

ences between narrowly spaced samples. These offsets are more likely to have resulted from sedimentary processes affecting the material that was dated.

[5] The main sedimentary processes concerned involve remobilization and redeposition of previously deposited materials and/or bioturbational mixing. Bioturbation effects have been previously discussed, in general [*Bard*, 2001] and for the specific example of *Zoophycos* burrows [*Löwemark and Werner*, 2001; *Bromley and Hanken*, 2003]. *Löwemark and Werner* [2001] emphasize that there can be considerable difficulty in recognising *Zoophycos* traces in unconsolidated sediments, and suggest that such burrows may cause age falsifications of as much as 1110–2525 years. These effects are not limited to the remobilization of older material by burrowing, but may also include the pushing of younger material down into older sediments by up to 1 m.

[6] Thus the real limitations to age accuracy are not instrumental but, determined by the nature of the dated materials and the sedimentary history. Datings on a single horizon are best viewed as individual samples from a probability function, which we aim to quantify here. The distribution of dates in previous work (see above) suggests that in the eastern Mediterranean as a whole, margins of ''error'' might be expected of the order of ±800 years.

[7] Our high-resolution Aegean records provide a unique opportunity to constrain a regional Aegean chronostratigraphic framework, by comparing and contrasting detailed multiproxy stratigraphic and AMS $^{14}$C data. With the Aegean's limited area it is expected that events would be (virtually) synchronous across the basin and the occurrence of the sapropel S1 provides a useful interval with suppressed bioturbation. We use a multiproxy approach to reduce parameter-specific bias, such as regional asynchroneity or patchiness in faunal records; postdepositional reoxygenation of sapropel tops [*Higgs et al.*, 1994; *Thomson et al.*, 1995]; or more general signal disturbances by, for example, bioturbation and reworking. An event-based stratigraphy enables the assembling of dates from several cores into a ''master'' stratigraphic framework with the potential to assess the error in any one individual dating. This allows

**Table 1.** Location of Cores and Regression Information

| Core | Location | Depth | Regression Coefficient, $r^2$ | Points | Equation |
|---|---|---|---|---|---|
| LC-21 | 35°40′N 26°35′E | 1522 m | - | - | - |
| SL-11 | 39°06′N 25°48′E | 258 m | 0.9835 | 9 | $y = 0.64x - 52.27$ |
| SL-21 | 39°01′N 25°25′E | 317 m | 0.9661 | 8 | $y = 0.49x - 24.53$ |
| SL-31 | 38°56′N 25°00′E | 430 m | 0.9743 | 9 | $y = 0.58x - 28.11$ |
| SLA-9 | 37°31′N 24°33′E | 260 m | 0.9809 | 9 | $y = 0.81x - 36.65$ |
| LC-31 | 35°00′N 31°10′E | 2298 m | 0.9599 | 10 | $y = 0.71x - 28.96$ |
| IN68-9 | 41°48′N 17°55′E | 1234 m | 0.9590 | 7 | $y = 0.82x - 66.96$ |
| C-40 | 36°56′N 24°05′E | 852 m | 0.9792 | 6 | $y = 0.70x - 29.43$ |
| SK-1 | 39°04′N 23°94′E | ~1000 m | 0.9837 | 6 | $y = 2.67x - 39.17$ |

insight into both temporal and spatial gradients. The event stratigraphic framework may provide further studies with a means to assess chronostratigraphy in considerable detail and hence to provide guidance for targeting new AMS radiocarbon datings.

## 2. Methods

[8] We present results for three gravity cores on a transect through the northern Aegean Basin (SL-11, SL-21, and SL-31), an additional gravity core (SLA-9) and two piston cores from the southern Aegean (LC-21) and from the Levantine Sea (LC-31). All six cores consist of microfossil-rich hemipelagic ooze with a clearly defined darker band of sapropelic material. Core locations are shown in Figure 1, with their exact coordinates and water depths detailed in Table 1.

[9] Each core was sampled in a contiguous sequence: SL-21, SL-31, and SLA-9 at 0.5 cm intervals; and LC-31 and LC-21 at 1 cm intervals for faunal analysis. Cores SLA-9, LC-21, and LC-31 were also sampled at 1 cm intervals for geochemical analysis. The faunal samples were freeze-dried, weighed, and selected (weighed) subsamples were disaggregated and wet sieved using demineralized water. The sieved fractions were collected on 600, 150, 125, and 63 $\mu$m mesh sizes. The >150 $\mu$m fractions were subdivided using a random splitter to provide an aliquot of at least 200 individual planktonic foraminifera, providing a significance level of at least 95% for species of 4% or greater relative abundance [see *Fatela and Taborda*, 2002]. These were then identified, sorted on Chapman slides, and counted. Results were recorded as absolute abundance in numbers $g^{-1}$ sediment dry weight and as relative abundance or percentages. We present here only the percentages, for brevity (Figure 2).

[10] Detailed stable oxygen and carbon isotope records have been constructed for several individual planktonic foraminiferal species in cores LC-21, LC-31, SLA-9, SL-11, SL-21, and SL-31, with resolutions of the order of 1 cm (Figure 3). The species selected were the shallow, surface-dwelling *Globigerinoides ruber* (white) and the deep-living species *Neogloboquadrina pachyderma* (right coiling) which has been associated with the Deep Chlorophyll Maximum at the base of the euphotic layer [*Rohling and Gieske*, 1989; *Rohling et al.*, 2004, 1995]. This selection follows global and specific Mediterranean habitat descriptions [*Hemleben et al.*, 1989; *Pujol and Vergnaud Grazzini*, 1995; *De Rijk et al.*, 1999; *Hayes et al.*, 1999; *Rohling et al.*, 1993, 1995, 1997, 2004], which are corroborated for the study area by isotopic evidence [*Casford et al.*, 2001, 2002]. The stable isotope analyses were performed at two separate intercalibrated facilities at the National Oceanography Centre (NOC) on a Europa Geo 20-20 with individual acid bath preparation; and at NERC Isotope Geoscience Laboratory (NIGL), Keyworth on the VG-Optima with a common acid bath preparation. Isotope results are reported in ‰ deviations from the Vienna Pee Dee Belemnite standard. Analytical errors are of the order of 0.06‰ ($1\sigma$).

[11] Samples for geochemical were freeze-dried, providing approximately 5g of dried material for analysis in LC-31 and 3g in SLA-9 and LC-21. Samples from cores LC-21 [see *Mercone et al.*, 2000] and LC-31 were analyzed by X-Ray Fluorescence (XRF) at NOC. The dried sample was ground in an agate mortar, then 3g was pressed into disc shaped pellets and the pellets analyzed for minor elements. The remaining 2g of material was treated with a fluxing agent and melted to form glass beads that were analyzed for major elements. Core SLA-9 was analyzed for concentrations of Al, S, Ba, Ca, Mn, Fe, and P by Induced Coupled Plasma - Optical Emission Spectroscopy (ICP-OES). Dried, ground samples were determined from digestion in a mixture of HF, $HNO_3$ and $HClO_4$ and final solution in 1 M HCl. This method is adapted from *Li et al.* [1995]. We note that the two methods can give significantly different values for certain elements, especially lithophiles, because of incomplete extraction.

## 3. Radiocarbon Dates

[12] AMS radiocarbon dates were obtained for cores LC-21, LC-31, SLA-9, and SL-31 using handpicked clean planktonic foraminiferal tests with no evidence of pyritization or overgrowth. The samples were too small for monospecific dating [*Bard et al.*, 1987], but no systematic differences would be expected within the Mediterranean basin for such dates relative to clean total planktonic foraminiferal tests [cf. *Jorissen et al.*, 1993]. The picked material was submitted for analysis at the NERC radiocarbon laboratory at SUERC (LC-21, LC-31) and at the Leibniz AMS Laboratory at Kiel (Germany) (SLA-9, SL-31). Datings for the other cores discussed here have been presented

**Figure 2.** Relative abundance of selected planktonic foraminifera with depth, for cores presented in this study. Circled numbers locate occurrence of primary faunal events (detailed in Table 3), and circled letters show locations of ancillary events (detailed in Table 4). The dark bar represents the position of the visible sapropel.

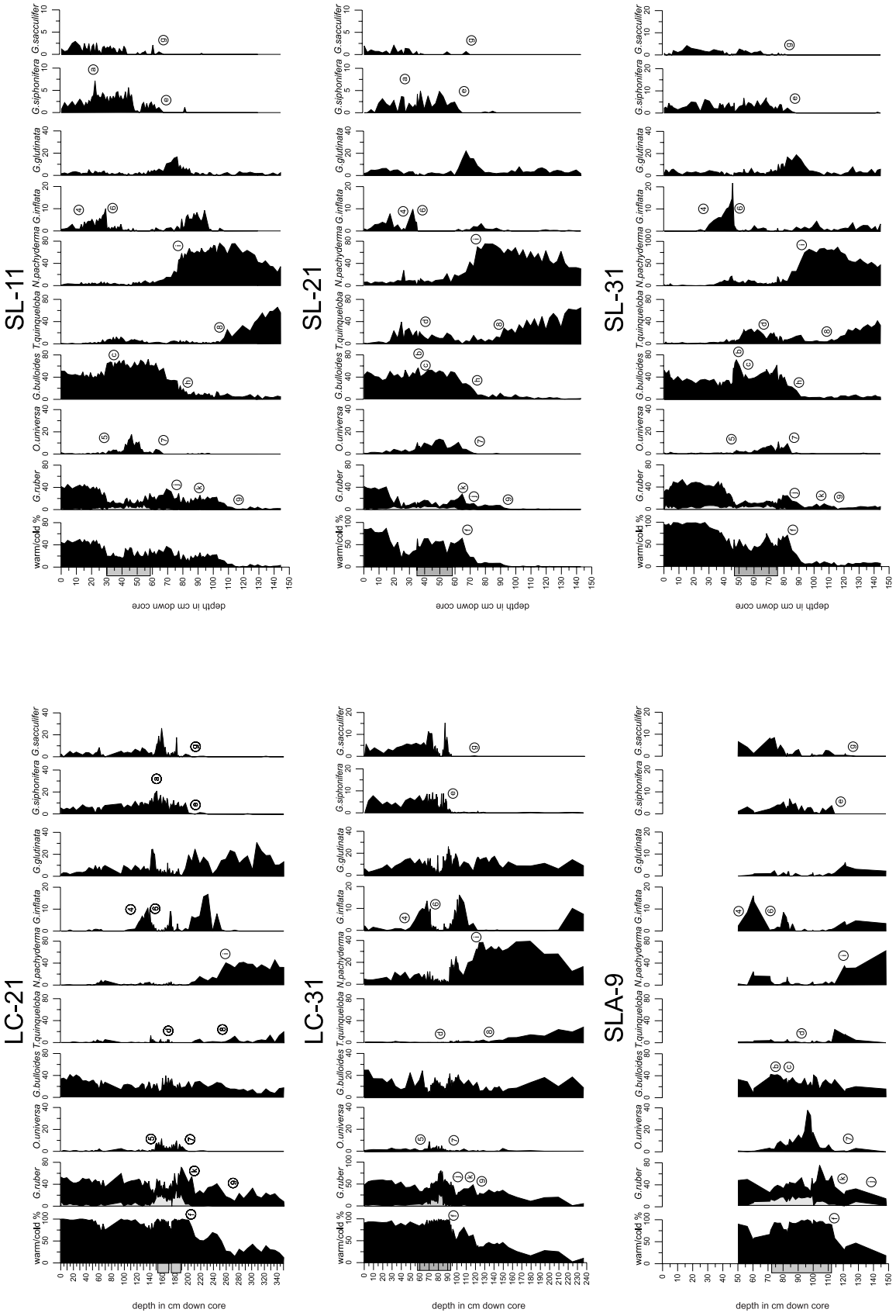
SL-11
SL-21
SL-31
LC-21
LC-31
SLA-9
G.sacculifer
G.siphonifera
G.glutinata
G.inflata
N.pachyderma
T.quinqueloba
G.bulloides
O.universa
G.ruber
warm/cold %
depth in cm down core

Figure 2

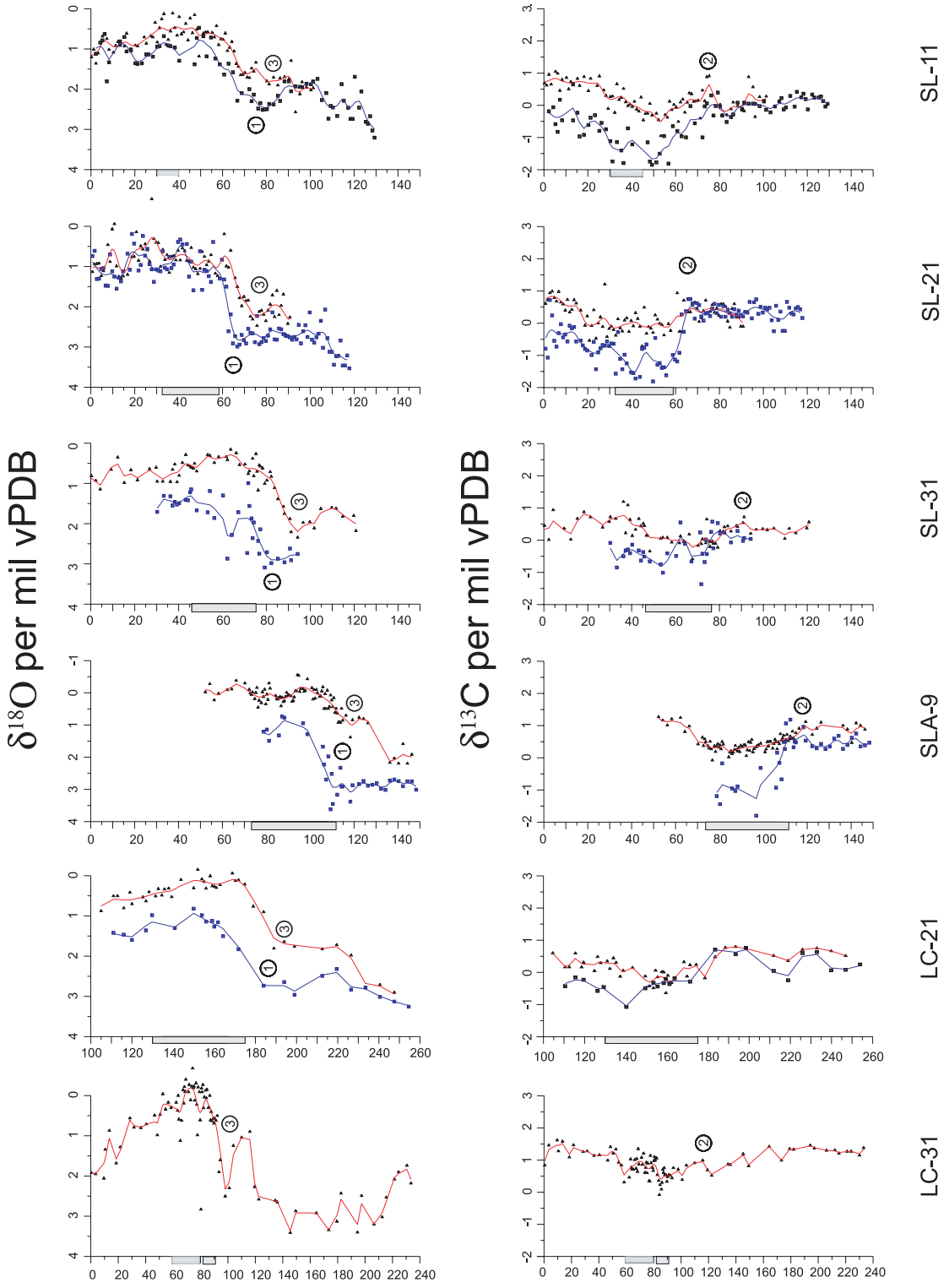


**Figure 3.** Stable isotope records for cores used in this study (for LC-21 see also *Casford et al.* [2002] and *Rohling et al.* [2002]). Triangles record the isotopic data from *G.ruber*, and the narrow line is a five point Gaussian smoothing of this data. Squares are data points, and the bold line indicate these same data points for *N.pachyderma*. Circled numbers indicate locations of primary isotopic events detailed in Table 3. The dark bar represents the position of the visible sapropel.

**Table 2.** Age Control Points Used in the Present Study, With True Depths in the Cores, and Corrected Depths (Subtracting Thickness of Turbidites and Ash Layers)[a]

| True Depth in Core, cm | Corrected Depth, cm | AMS Laboratory Code | Uncorrected AMS $^{14}$C Age From Direct Dating or Dated Horizon, ka B.P. | Sedimentation Rate, cm ka$^{-1}$ | Sample Range, cm | Bioturbation Uncertainty, cm | Correlation Error, 1 SE, cm | Sampling Uncertainty, years | Total Uncertainty, years | 2$\sigma$ Lower Cal Range years B.P. | 2$\sigma$ Upper Cal Range years B.P. | Median Age, Cal $^{14}$C years B.P. |
|---|---|---|---|---|---|---|---|---|---|---|---|---|
| | | | | | *LC-21* | | | | | | | |
| 50 | 50 | CAMS-41314 | 3.35 ± 0.06 | 21.1 | 1 | 10 | 0 | 521 | 581 | 1946 | 4380 | 3139.5 |
| 95.5 | 85.5 | CAMS-41313 | 4.29 ± 0.06 | 21.1 | 1 | 10 | 0 | 521 | 581 | 3146 | 5558 | 4328.5 |
| 137.75 | 127.75 | CAMS-41311 | 5.59 ± 0.06 | 21.1 | 1 | 10 | 0 | 521 | 581 | 4780 | 7050 | 5905.5 |
| 161.5 | 151.5 | CAMS-41315 | 7.48 ± 0.06 | 21.1 | 1 | 10 | 0 | 521 | 581 | 7630 | 7951 | 7794.5 |
| 174.25 | 164.25 | CAMS-41312 | 8.12 ± 0.06 | 21.1 | 1 | 1 | 0 | 95 | 155 | 8266 | 8620 | 8437.5 |
| 179.5 | 169.5 | AA-30364 | 9.01 ± 0.07 | 21.1 | 1 | 1 | 0 | 95 | 165 | 9329 | 9788 | 9530.5 |
| 209 | 199 | AA-30365 | 11.77 ± 0.08 | 21.1 | 1 | 10 | 0 | 521 | 601 | 11,885 | 14,495 | 13,218 |
| 252.5 | 242.5 | CAMS-41316 | 14.45 ± 0.06 | 21.1 | 1 | 10 | 0 | 521 | 581 | 15,329 | 18,151 | 16,752 |
| | | | | | *LC-31* | | | | | | | |
| 28.5 | 28.5 | CAMS-45864 | 3.45 ± 0.05 | 10.9 | 0.5 | 10 | 9.3 | 963 | 1867 | 0 | 6791 | 3468.5 |
| 60.5 | 60.5 | CAMS-45863 | 6.12 ± 0.05 | 10.9 | 0.5 | 10 | 9.3 | 963 | 1867 | 2141 | 10,513 | 6387 |
| 87.5 | 82.5 | CAMS-45861 | 8.74 ± 0.05 | 10.9 | 0.5 | 1 | 9.3 | 138 | 1041 | 7166 | 11,755 | 9303 |
| 96.5 | 91.5 | CAMS-45862 | 8.50 ± 0.05 | 10.9 | 0.5 | 1 | 9.3 | 138 | 1041 | 6819 | 11,301 | 9025 |
| 131.5 | 126.5 | CAMS-45860 | 12.04 ± 0.05 | 10.9 | 0.5 | 10 | 9.3 | 963 | 1867 | 9251 | 18,187 | 13,596 |
| 247.5 | 242.5 | CAMS-45859 | 32.96 ± 0.05 | 10.9 | 0.5 | 10 | 9.3 | 963 | 1867 | | | |
| | | | | | *SL-31* | | | | | | | |
| 45.75 | 45.75 | KIA9467 | 6.52 ± 0.05 | 8.6 | 0.5 | 10 | 6.8 | 1221 | 2062 | 2126 | 11425 | 6869 |
| 59.75 | 59.75 | KIA9468 | 7.95 ± 0.06 | 8.6 | 0.5 | 1 | 6.8 | 174 | 1025 | 6388 | 10513 | 8395 |
| 78.25 | 78.25 | KIA9469 | 9.33 ± 0.06 | 8.6 | 0.5 | 10 | 6.8 | 1221 | 2072 | 5681 | 15117 | 10252 |
| 85 | 85 | KIA9470 | 9.99 ± 0.06 | 8.6 | 0.5 | 10 | 6.8 | 1221 | 2072 | 6438 | 15966 | 11035 |
| 120.25 | 120.25 | KIA9471 | 14.65 ± 0.08 | 8.6 | 0.5 | 10 | 6.8 | 1221 | 2092 | 11,291 | 20936 | 16394 |
| | | | | | *SLA-9* | | | | | | | |
| 60.5 | 60.5 | KIA9472 | 5.95 ± 0.05 | 12.5 | 0.5 | 10 | 7 | 840 | 1450 | 2932 | 9306 | 6202 |
| 71.5 | 71.5 | KIA9473 | 6.45 ± 0.05 | 12.5 | 0.5 | 10 | 7 | 840 | 1450 | 3501 | 9947 | 6783 |
| 83.25 | 83.25 | KIA9474 | 7.90 ± 0.05 | 12.5 | 0.5 | 1 | 7 | 120 | 730 | 6906 | 9805 | 8302.5 |
| 99.5 | 99.5 | KIA9475 | 8.40 ± 0.05 | 12.5 | 0.5 | 1 | 7 | 120 | 730 | 7492 | 10367 | 8858 |
| 120.5 | 120.5 | KIA9476 | 11.91 ± 0.07 | 12.5 | 0.5 | 10 | 7 | 840 | 1470 | 9788 | 16991 | 13401 |
| | | | | | *C-40* | | | | | | | |
| 73.5 | 73.5 | Beta-110420 | 6.83 ± 0.11 | 14.1 | 1 | 10 | 9.5 | 780 | 1564 | 5469 | 8783 | 7127 |
| 82.5 | 82.5 | Beta-110419 | 7.83 ± 0.14 | 14.1 | 1 | 1 | 9.5 | 142 | 956 | 6612 | 10052 | 8240 |
| 131 | 131 | Beta-110418 | 12.35 ± 0.16 | 14.1 | 1 | 10 | 9.5 | 780 | 1614 | 10,396 | 17802 | 14003 |
| | | | | | *SK-1* | | | | | | | |
| 143.5 | 143.5 | | 3.81 ± 0.10 | 58.5 | 1 | 10 | 32.2 | 188 | 838 | 1968 | 5550 | 3732.5 |
| 284 | 284 | | 6.58 ± 0.07 | 58.5 | 1 | 1 | 32.2 | 34 | 655 | 5627 | 8019 | 6876.5 |
| 524 | 524 | | 9.64 ± 0.08 | 58.5 | 1 | 1 | 32.2 | 34 | 665 | 8720 | 12417 | 10509 |
| 690 | 690 | | 13.43 ± 0.13 | 58.5 | 1 | 10 | 32.2 | 188 | 868 | 13,345 | 17307 | 15291 |
| | | | | | *IN68-9* | | | | | | | |
| 11.5 | 7.5 | UTC-500 | 3.16 ± 0.12 | 9.5 | 0.5 | 10 | 14.2 | 1105 | 2720 | 0 | 8099 | 3578 |
| 54.5 | 38.5 | UTC-1607 | 6.39 ± 0.06 | 9.5 | 0.5 | 1 | 14.2 | 158 | 1713 | 2753 | 10340 | 6599 |
| 157.25 | 81.25 | UTC-501 | 9.28 ± 0.18 | 9.5 | 0.5 | 1 | 14.2 | 158 | 1833 | 6289 | 13816 | 10052 |
| 241.5 | 157.5 | UTC-502 | 13.10 ± 0.20 | 9.5 | 0.5 | 10 | 14.2 | 1105 | 2800 | 8480 | 20827 | 14917 |

**Table 2.** (continued)

| True Depth in Core, cm | Corrected Depth, cm | AMS Laboratory Code | Uncorrected AMS $^{14}$C Age From Direct Dating or Dated Horizon, ka B.P. | Sedimentation Rate, cm ka$^{-1}$ | Sample Range, cm | Bioturbation Uncertainty, cm | Correlation Error, 1 SE, cm | Sampling Uncertainty, years | Total Uncertainty, years | 2$\sigma$ Lower Cal Range years B.P. | 2$\sigma$ Upper Cal Range years B.P. | Median Age, Cal $^{14}$C years B.P. |
|---|---|---|---|---|---|---|---|---|---|---|---|---|
| 322.5 | 201.5 | UTC-503 | 14.20 ± 0.30 | 9.5 | 0.5 | 10 | 14.2 | 1105 | 2900 | 9470 | 22018 | 15812 |
| 510.5 | 247.5 | UTC-504 | 17.20 ± 0.30 | 9.5 | 0.5 | 10 | 14.2 | 1105 | 2900 | 14,075 | 25580 | 19864 |

[a]Samples with codes starting CAM were prepared as graphite targets at the NERC radiocarbon laboratory and analyzed at the Lawrence Livermore National Laboratory Accelerator Mass Spectrometry (AMS) facility. Sample codes AA were prepared at Scottish Universities Reactor Research Centre at East Kilbride and analyzed at the Arizona Radiocarbon Facility. KIA sample codes indicate the Leibniz AMS Laboratory at Kiel. Radiocarbon convention ages were calibrated using marine mode of programme Calib5.1 [*Stuiver and Reimer*, 1993; *Stuiver et al.*, 1998]. Cores LC-21, LC-31, SL-31, SLA-9, C-40, and SK-1 datings include a local $\Delta$R correction of 149 ± 39 years [*Facorellis et al.*, 1998] in the sapropel and a $\Delta$R of 58 ± 85 years [*Reimer and McCormac*, 2002] outside of the sapropel; see text for further discussion. Dates in LC-21 are after *Mercone et al.* [2000], and dates in C-40 are after *Geraga et al.* [2000]. Sedimentation rates are determined from the known radiocarbon dates in each core, and a mean sedimentation rate is used in each core. Sample uncertainty is calculated as the sum of the uncertainties in sample range and in possible bioturbation range (see text). Total uncertainties include the sampling uncertainty, the stated AMS machine errors, and the uncertainty in the correlation framework used to transpose these dates into the stacked time frame. Calibrated age range is given as the 2 sigma range after [*Stuiver and Reimer*, 1993; *Stuiver et al.*, 1998], and the median probability age is also given [*Stuiver and Reimer*, 1993; *Stuiver et al.*, 1998].

previously: cores SK-1 [*Zachariasse et al.*, 1997], IN68-9 [*Jorissen et al.*, 1993; *Rohling et al.*, 1997], and C-40 [*Geraga et al.*, 2000]. We calibrate radiocarbon ages in this paper using the IntCal Marine04 curve and the program Calib 5.1 [*Stuiver and Reimer*, 1993, *Hughen et al.*, 2004a] with reservoir-age corrections ($\Delta$R) as discussed in the text.

[13] Radiocarbon datings are best seen as a direct expression of the concentration of $^{14}$C (abbrv. [$^{14}$C]). As such, they contain three components: the age-controlled reduction in [$^{14}$C] from original concentrations common in all cores; a reservoir age effect, which for any given time slice is likely to be very similar in the cores presented here because of their close proximity; and an undetermined contribution of old carbon, which may vary considerably between individual core samples. The radiocarbon convention ages obtained are shown in Table 2. To obtain reliable calibrated ages, an accurate assessment of the reservoir age effect and of the calibration to calendar years is needed. Both of these require foreknowledge of the error in the undetermined old carbon contribution, with small increases in the uncertainty of uncorrected ages adding considerably to the errors in calibrated ages. Here, we present two direct date comparisons using uncalibrated ages and calibrated ages both constrained by basinwide synchronous events. This event stratigraphy allows us to produce a reduced error age model for uncalibrated and calibrated radiocarbon concentrations in the eastern Mediterranean. These two approaches are complementary to one another. The uncalibrated age model makes no assumption of error size, and so provides an independent assessment of the size of the total uncertainty, but it is based on the assumption that reservoir age effects are similar between cores (see section 7). The calibrated model allows us to directly assess the component causes of uncertainty in individual samples, but requires that we make assumptions about the size of these uncertainties before calibrating the dates. Together these two approaches allow us to assess the potential errors in both the dating and calibration process.

## 4. Event Stratigraphy

[14] We identify and describe 24 faunal, isotopic and geochemical events and use these to define a stratigraphically controlled chronology. Each event is identified by either a sharp change in gradient with time or by alternations of presence and absence in the case of faunal changes. We divide these events into 12 primary and 12 ancillary events. The primary events are defined as occurring in all cores (analysis permitting) and appear to be basin wide. Ancillary events (mostly faunal) are defined as those that occur only in some of the cores and/or those that may have the potential to give a local or asynchronous expression.

[15] Primary events are subdivided into isotopic, faunal, and chemical. These are detailed, together with the depth of occurrence, by core, in Table 3. The three primary isotope events were defined as occurring at the point of inflection for the major gradient changes (see Figure 3). We recognize (event 1) the inflection in the *N.pachyderma* $\delta^{18}$O depletion immediately below base of the sapropel; (event 2) the high point at the shoulder of the $\delta^{13}$C *G.ruber* depletion sited

**Table 3.** Depth Occurrence of Primary Events by Core[a]

| Number | Primary Events | LC-21, Correlated | SL-11 | SL-21 | SL-31 | SLA-9 | LC-31 | IN-689 | C-40 | SK-1 |
|---|---|---|---|---|---|---|---|---|---|---|
| | | | | | *Isotopes* | | | | | |
| 1 | $\delta^{18}$O *N.pachyderma* inflection below sapropel | 186.5 | 66.75 | 66.75 | 82.75 | 109.25 | - | - | - | - |
| 2 | $\delta^{13}$C *G.ruber* high before depletion into sapropel | 186.5 | 74.25 | 60.75 | 82.25 | 119.25 | 106.5 | - | - | - |
| 3 | $\delta^{18}$O *G.ruber* inflection below sapropel | 191.5 | 68.25 | 75.75 | 91.75 | 112.75 | 101.5 | 86.5 | - | - |
| | | | | | *Fauna* | | | | | |
| 4 | exit/low in *G.inflata* above sapropel | 106.5 | 22.25 | 27.25 | 28.75 | 50.25 | 49.5 | 27.5 | 40.0 | 271.0 |
| 5 | exit/low in *O.universa* above sapropel | 137.0 | 29.25 | - | 46.25 | - | 59.5 | 37.5 | 65.0 | 300.0 |
| 6 | last entrance of *G.inflata* in the top of the sapropel | 131.0 | 30.25 | 35.25 | 52.75 | 68.25 | 71.75 | 47.5 | 70.5 | 293.0 |
| 7 | exit/low in *O.universa* below sapropel | 190.5 | 67.25 | 74.75 | 85.25 | 121.75 | - | 71.5 | 102.5 | 486.0 |
| 8 | exit/end of *T.quinqueloba* ramp down | 242.0 | 104.25 | 89.75 | 108.75 | - | 134.5 | 141.5 | 131.0 | 622.0 |
| 9 | last distinct low in *G.ruber* (T1a?) | 263.0 | 117.25 | 102.25 | 121.75 | - | 172.5 | 149.5 | 160.5 | 648.0 |
| | | | | | *Chemistry* | | | | | |
| 10 | top of Barium anomaly | 120.5 | - | - | - | 60.5 | 60.0 | - | - | - |
| 11 | lowest point in Barium saddle | 153.0 | - | - | - | 82.5 | 84.0 | - | - | - |
| 12 | base of Barium anomaly | 188.5 | - | - | - | 113.5 | 99.0 | - | - | - |

[a]Units are centimeters.

around the onset of the sapropel; and (event 3) the inflection in $\delta^{18}$O *G.ruber*, marking the start of the depletion sited immediately below base of the sapropel (T1b). This final isotope event is similar in character to isotope event 1. However, it appears to occur earlier than the $\delta^{18}$O *N.pachyderma* inflection. The nature and causes of these events are examined in more detail by *Casford et al.* [2002, 2003].

[16] Faunal events are identified on exits, entries and particularly strong inflections in the faunal record. Both absolute and relative abundance records were used to establish the exact levels of entries and exits. Inflections in the record were taken from relative abundance plots only and may reflect population shifts rather than changes in absolute numbers of the individual species listed. The primary faunal events (Figure 2 and Table 3) are (event 4) the exit or low in *G.inflata* above peak at top of sapropel; (event 5) the first (near) absence of *O.universa* above the sapropel; and (event 6) the minimum or absence in *G.inflata* near the top of the sapropel, which is followed by a rapid increase in *G.inflata* on or shortly after the top of the darker sapropelic material. Next, we use (event 7) the last absence of *O.universa* before the sapropel; (event 8) the end of the ramping down in *T.quinqueloba* relative abundance below the sapropel, which often ramps down to zero abundance; and (event 9) the first, rapid increase in *G.ruber* located below the sapropel, marking the shift from very low values or absence to the higher Holocene/sapropel levels. This population shift seems to be associated with the isotopic increase in $\delta^{18}$O *G.ruber* normally identified as Termination 1a [*Casford et al.*, 2001, 2002]. This faunal point is constrained at the last low value in *G.ruber*'s relative abundance before the increase.

[17] Chemical signals in marine cores generally record diagenetic changes within the sediment. This is a particular problem during periods of sapropel deposition which are known to suffer oxidative "burn down". This study focuses on the barium signal, as while there is some potential for remobilization [*Dickens*, 2001], the Ba/Al ratio is widely believed to reflect precipitation associated with primary productivity or at least to record syndepositional changes (further discussion by *Calvert* [1983]; *Van Os et al.* [1991, 1994]; *Thomson et al.* [1999]; and *Mercone et al.* [2001]). These primary geochemical events are identified by their deviation from background values, as shown in Figure 4: (event 10) the end of Ba/Al anomaly, where it returns to background values; (event 11) the lowest point in the saddle in the Ba/Al anomaly within the sapropel and; (event 12) the start of the anomaly, where the Ba/Al ratio appears to depart from background values.

[18] Ancillary events are identified in Table 4 and illustrated in Figures 2 and 3. We determine the regression relationships between the depths of occurrence of the primary events in each core, to allow a direct stratigraphically controlled comparison between the cores. The details of each regression are given in Table 1, and we show the ±2 standard errors (SE) interval relevant for each regression on the plots (Figure 1). The ancillary events are also provided in these plots as validation of the primary regression. As core LC-21 is one of the best dated and most understood records in the eastern Mediterranean [*Hayes et al.*, 1999; *De Rijk et al.*, 1999; *Mercone et al.*, 2000, 2001; *Casford et al.*, 2002; *Rohling et al.*, 2002; *Casford et al.*, 2003], we use LC-21 as the standard and we plot the occurrence depth of all events in each individual core versus their equivalent depths in LC-21.

[19] The statistically determined multiproxy stratigraphic framework allows the production of "stacked" age models, using the regression equations, to project both uncalibrated and calibrated AMS $^{14}$C datings from the various records (Table 2) onto the age-depth framework of LC-21. We already have a well-constrained chronostratigraphic framework for LC-21 from its "own" AMS $^{14}$C datings (Table 2) and by correlation to GISP II [*Rohling et al.*, 2002], so we can use the ages projected from other cores to assess the quality of our intercore (radiocarbon) correlations. The 2 SE intervals constrain the uncertainty in the assigned LC-21 equivalent depths. If this projection were poor, the dates from the other Aegean cores would be unlikely to fit within the established time framework. Having thus projected all datings into LC-21, the new joint dating framework can be compared against the framework on the basis of the datings for LC-21 proper (Figure 5). We conclude that our correla-

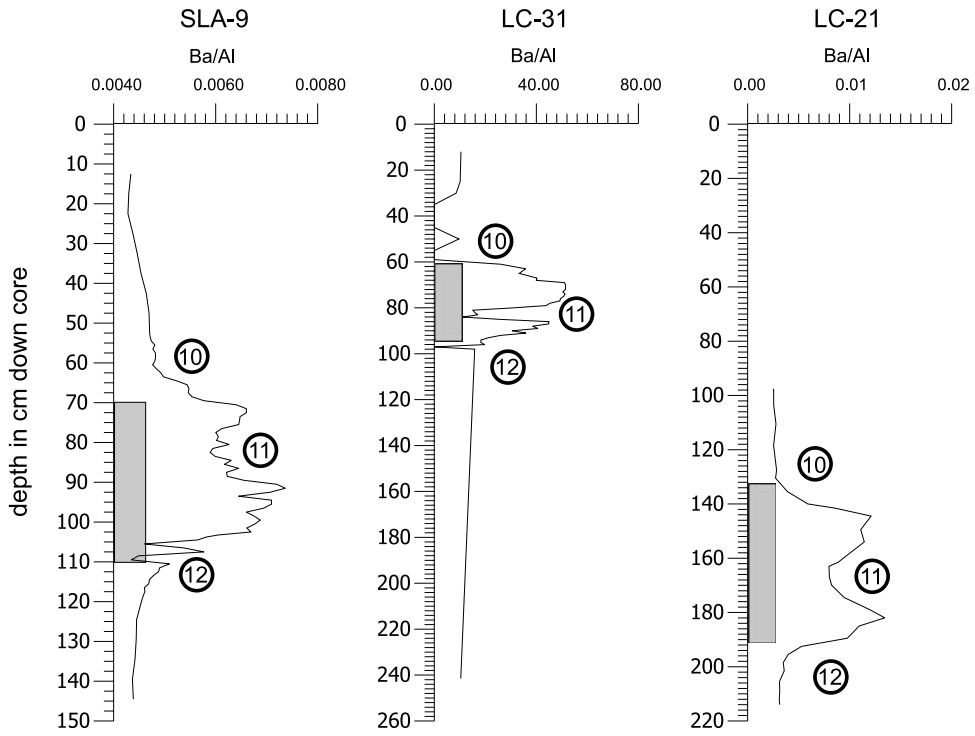


**Figure 4.** Concentration of barium in bulk sediment, expressed as the ratio Ba/Al, for cores in this study (see also *Mercone et al.* [2001] for LC-21). Circled numbers indicate primary geochemical events (Table 3). The dark bar represents the position of the visible sapropel. We note that the Ba/Al ratio differs significantly between the cores; this may relate to differences in analytical techniques, local productivity, clay inputs, or a combination of these.

tion model is robust. In addition, the age-depth model for LC-21 can thus be corroborated and further detailed by the addition of the projected datings from our correlated cores.

## 5. Uncalibrated Chronology

[20] We use the new composite Aegean time frame to examine other previously published, lower-resolution records from the same region: cores SK-1 [*Zachariasse et al.*, 1997] and C-40 [*Geraga et al.*, 2000]. These are located close to our existing cores (Figure 1), provide good signal comparability with our records and allow the assumption that reservoir ages between cores are small [*Reimer and McCormac*, 2002] (see discussion of calibrated framework in section 6). Any differences in the reservoir ages will be constrained within the 2 SE correlation uncertainty. The depth of each identified correlation level in these cores is listed in Table 3 and regressions are shown in Figure 6. The equations for standardizing depths to the LC-21 depth scale are shown in Table 1, and these were used to calculate the

**Table 4.** Depth Occurrence of Ancillary Events by CORe[a]

| Number | Ancillary Events | LC-21, Correlated | SL-11 | SL-21 | SL-31 | SLA-9 | LC-31 | IN-689 | C-40 | SK-1 |
|---|---|---|---|---|---|---|---|---|---|---|
| a | peak in *G.siphonifera*. | - | 22.25 | 26.25 | 30.25 | - | | | | |
| b | *G.bulloides* peak in sapropel | - | 29.25 | 34.75 | 47.25 | 71.25 | | | 73.0 | 304.5 |
| c | low before *G.bulloides* peak | - | 34.25 | 37.25 | 53.25 | 80.25 | | | 76.5 | 314.0 |
| d | start of *T.quinqueloba* pick-up in sapropel | 160.5 | | 42.25 | 60.25 | - | | | 89.5 | 402.0 |
| e | last exit of *G.siphonifera* before sapropel | 200.5 | 67.25 | 64.75 | 88.25 | 114.25 | | | 98.5 | 486.0 |
| f | drop in warm/cold plot below sapropel | 190.5 | | 64.75 | 88.25 | 112.25 | | | 95.0 | 520.0 |
| g | last exit of *G.sacculifer* below sapropel | 195.5 | 66.25 | 67.25 | 80.25 | 128.25 | | | 102.5 | 565.0 |
| h | *G.bulloides* low | - | 77.25 | 74.25 | 91.25 | - | | | 120.5 | 543.0 |
| i | shoulder of drop in *N.pachyderma* | 249.0 | 77.25 | 74.75 | 92.5 | - | | | 120.5 | 571.0 |
| j | last absence of *G.ruber rosa* below sapropel | 195.5 | 78.25 | 74.75 | 91.25 | - | | | - | 543.0 |
| k | first occurrence of *G.ruber rosa* before sapropel | 228.0 | 96.25 | 72.25 | 106.75 | - | | | - | 555.0 |
| l | midpoint of initial $\delta^{18}$O *N.pachyderma* depletion (T1a) | - | 105.75 | 108.5 | 120.0 | - | | | - | - |
| | top of dark layer | 131.0 | 30.25 | 35.25 | 46.75 | 73.0 | | | | |
| | base of dark layer | 174.5 | 58.75 | 58.5 | 77.5 | 112.25 | | | | |

[a]The final events listed are for reference only and were not used in the regression. Units are centimeters.

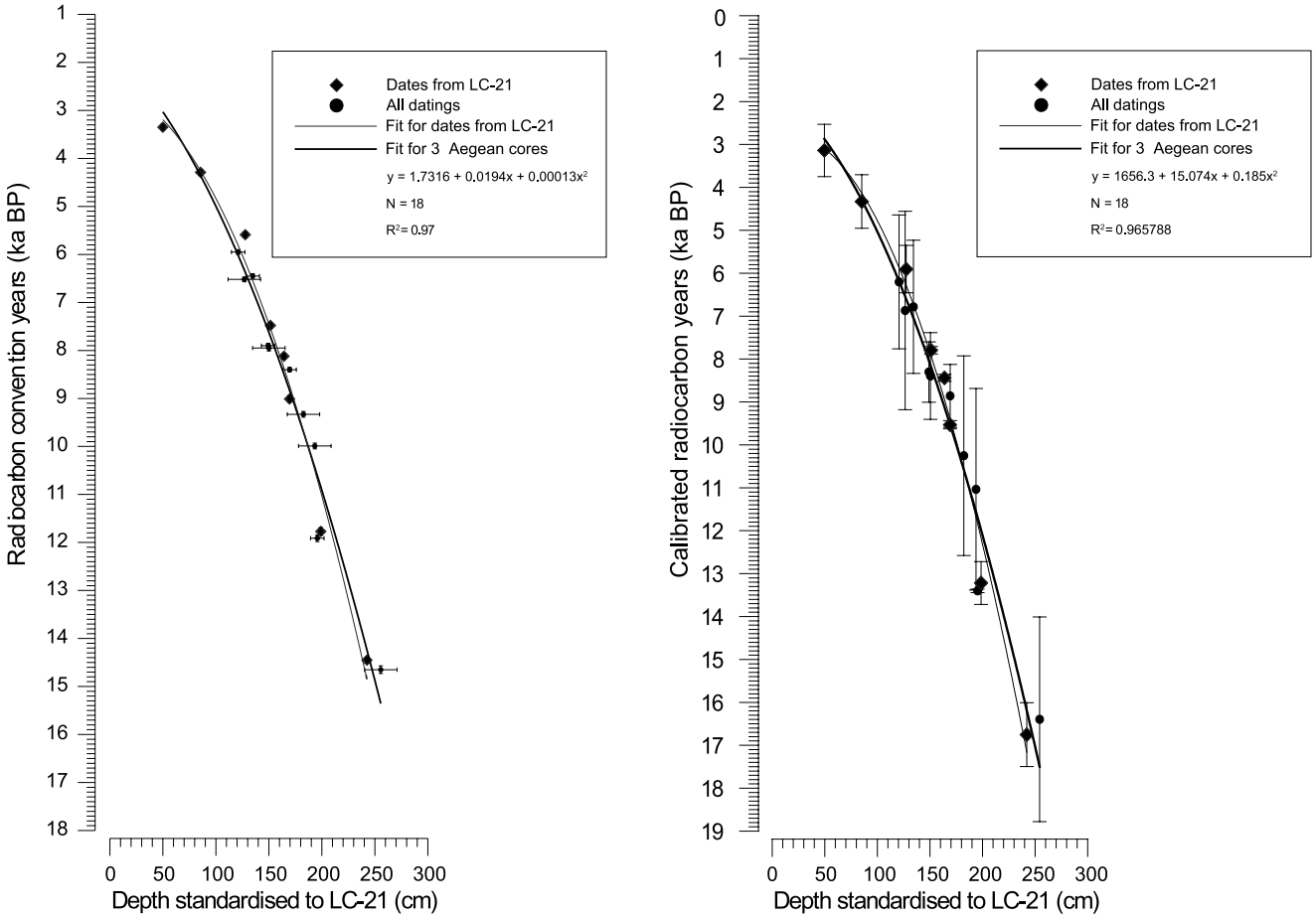


**Figure 5.** Chronostratigraphic framework for LC-21 and all dated Aegean cores from this study, showing radiocarbon convention ages and calibrated ages from our Aegean cores plotted versus a LC-21 equivalent depth. The narrow line indicates best fit regression for datings on LC-21 only, and the heavy line indicates the best fit regression on our three Aegean Sea cores. For radiocarbon convention ages the vertical error bars represent the machine errors quoted for the datings (see Table 2) and horizontal error bars equate to the 2 SE from our "event occurrence versus depth" regressions, projected on a LC-21 equivalent depth scale. For calibrated ages, only vertical error bars are shown as all uncertainties must be estimated before calibration. The size of these bars represents the 1 sigma probability spread of the calibration, with median values for the date shown as symbol points. In addition, we detail the second-order polynomial for all Aegean datings, shown within the legend.

LC-21 equivalent depths for the datings in cores SK-1 and C-40, reported in the source publications. Figure 6 shows these dates against the Aegean framework of "age versus LC-21 equivalent depth" that was presented in Figure 5.

[21] We also examine the potential use of our method in cores from outside the Aegean Sea. Two high-resolution cores were chosen: LC-31 (Levantine/eastern Mediterranean Sea; this study) and IN68-9 (Adriatic Sea [*Jorissen et al.*, 1993; *Rohling et al.*, 1997]). These cores were selected, as both possess multiproxy records and AMS radiocarbon datings. The identified events are detailed in Table 2 and the regressions are shown in Figure 6 and itemized in Table 1. As with SK-1 and C-40, we plot these cores' AMS $^{14}C$ datings versus LC-21 equivalent depth (based on the regressions), in comparison with our overall Aegean framework (Figure 5). The result provides strong endorsement of our new correlation method and of our overall Aegean chronostratigraphic framework, hence con-

**Figure 6.** The extended, eastern Mediterranean chronostratigraphic framework including the additional datings from C-40, Sk-1, LC-31, and IN68-9 against the regression for our three Aegean cores from Figure 5. Event occurrence regressions are included to the right of the age correlation, with regressions of the depth occurrence (in centimeters down core) for primary events (solid diamonds) and ancillary events (open diamonds) and a 2 SE error bar on the *x* axis.

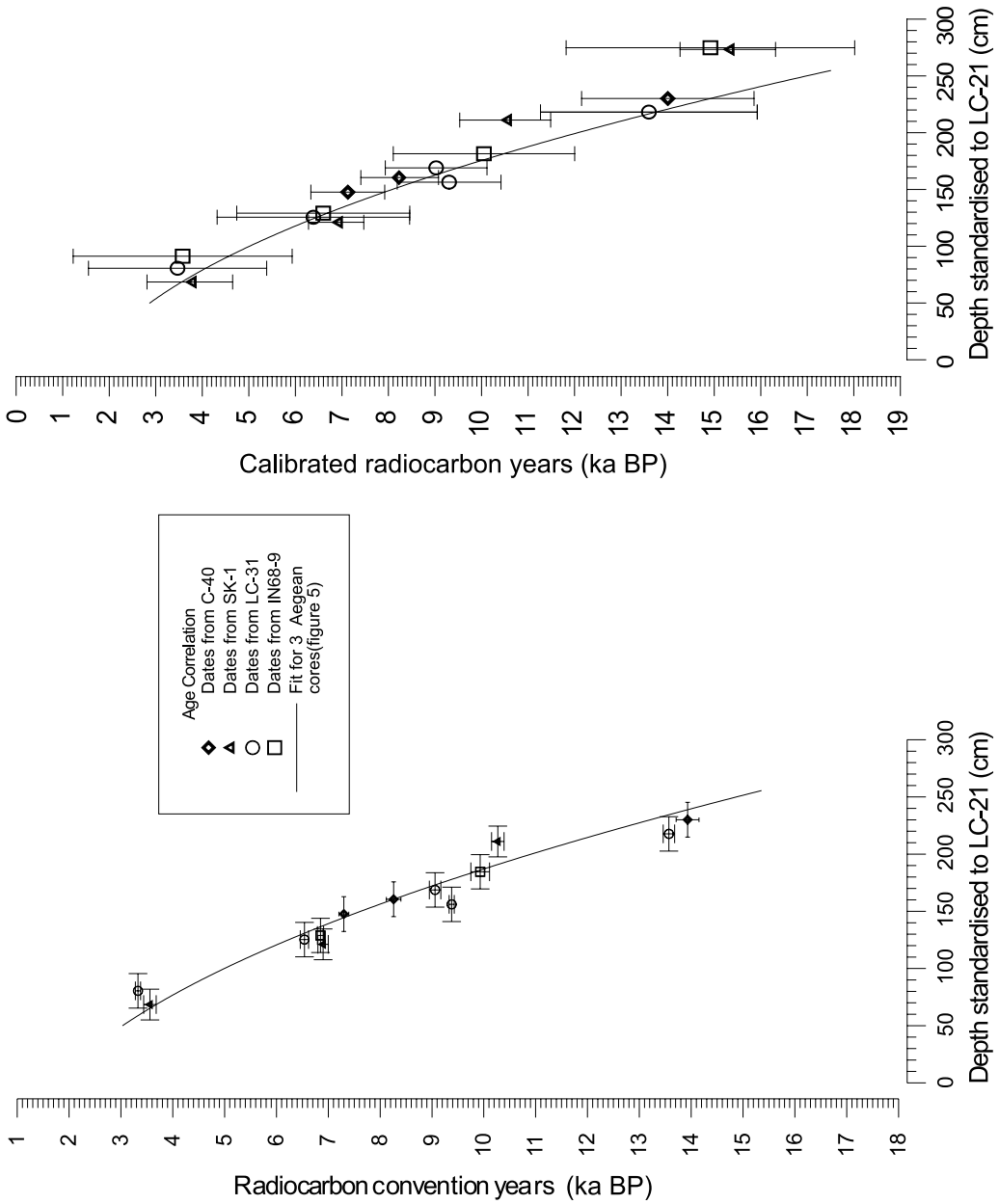
Calibrated radiocarbon years (ka BP)
Depth standardised to LC-21 (cm)
Radiocarbon convention years (ka BP)
Depth standardised to LC-21 (cm)
Age Correlation
Dates from C-40
Dates from SK-1
Dates from LC-31
Dates from IN68-9
Fit for 3 Aegean cores(figure 5)

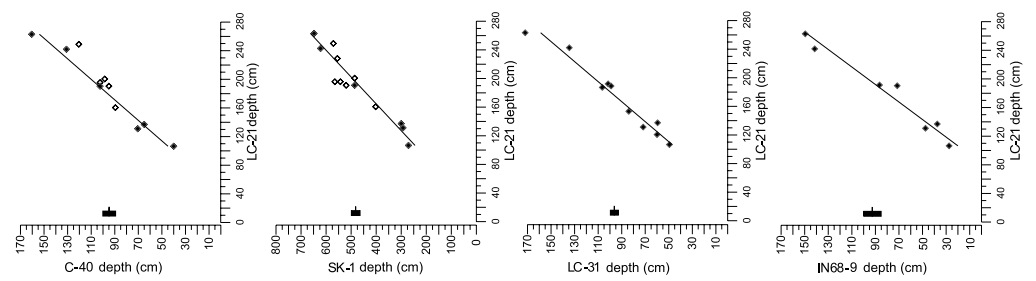
C-40 depth (cm)
SK-1 depth (cm)
LC-31 depth (cm)
IN68-9 depth (cm)
LC-21 depth (cm)

**Figure 6**

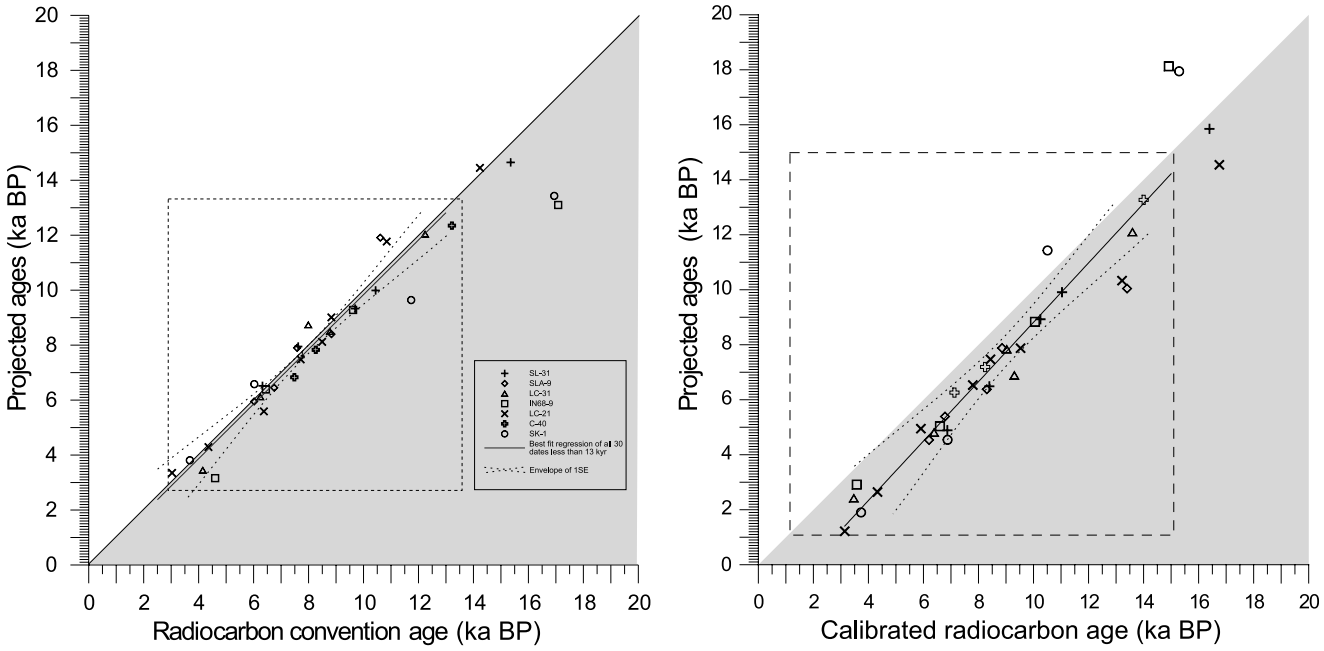


**Figure 7.** Evaluation of the overall time stratigraphic framework, showing all Accelerator Mass Spectrometry (AMS) datings (radiocarbon convention and calibrated ages) plotted versus their equivalent predicted age from the event stratigraphy, determined from their LC-21 standardized depth and projected on our three Aegean core chronostratigraphic framework. The dashed box shows the extent of the area constrained by our depth occurrence regressions, and the shaded area indicates the ''fall'' direction expected for older datings. The heavy line indicates the ''best fit'' linear regression for all AMS datings younger than 14 ka B.P. (i.e., those that fall within our correlatable boundaries), and the lighter weight line shows our projected 45° ideal fit.

firming that the framework is also applicable outside the Aegean Sea.

[22] To evaluate the usefulness of our method and the resultant Aegean (and eastern Mediterranean) chronostratigraphic framework (Figure 5), a critical quantitative assessment is needed. Using our chronostratigraphic framework an age can be predicted for each depth in LC-21, and therefore via the regressions, in any of the correlated cores. We can thus predict an age for all horizons at which AMS $^{14}$C datings were performed. In an ideal case the predicted and analyzed values would coincide perfectly, and a plot of one versus the other (Figure 7) would follow a 45° line through the origin. Since most conceivable mechanisms biasing AMS ages tend to impose shifts toward older values, we expect a proportion of the datings to fall off the isoline toward older ages (shaded area). Figure 7 shows an excellent overall agreement between predicted and observed ages, even in datings that are entirely independent of the time frame used for the predictions (i.e., those in LC-31, IN68-9, C-40, and SK-1).

[23] Using the age in radiocarbon convention years, the isoline falls within 1 SE (~120 years) of the regression through all points (Figure 7). Within our ability to determine, these lines appear to be identical. The framework must then approach the chronostratigraphic accuracy of the dating technique itself and the spread of datings around this line will reflect the total (analytical plus material related) error of the individual AMS datings, including any potential variation in $\Delta$R between sites. This suggests that the total error for AMS $^{14}$C datings on this type of material is of the order of ±240 years (2 SE) in the eastern Mediterranean.

## 6. Calibrated Framework

[24] We can follow the same process with the calibrated datings. However, before this is possible we must have a clear understanding of the size of potential errors in this process and the value for the marine carbon reservoir age. Any direct intercomparison of dating between cores requires radiocarbon dates to be corrected for variations in production rates of $^{14}$C over time (calibration), the contribution of old carbon, and to account for the marine reservoir effect.

[25] Unlike the uncalibrated datings we need to determine the sample uncertainty and reservoir ages directly before we can accurately calibrate the dates. To do this we need to know the size of contribution of old carbon. However, until technology advances enough to allow dating on single foraminifera these measurements can only be estimated. For the cores in this study we assume bioturbation to be limited to 10 cm [*Casford et al.*, 2002] except within the periods of sapropel deposition [*Rohling et al.*, 2002]. During sapropel deposition bioturbation appears to be reduced. Only few sapropels are truly laminated, however, so in most cases there may have been some bioturbation,

and an estimate of 1 cm homogenization is used in these periods. Similarly the sampling interval (an integration of several decades to centuries) will also add to the uncertainty. These sampling uncertainties together with the analytical uncertainty are detailed in Table 2. A simple addition of these errors suggests the uncertainties in any one dating may be as large as 1200 years and is termed sampling uncertainty in Table 2, i.e.,

$$\delta_{\text{sampling uncertainty}} = \sqrt{\left(\delta^2_{\text{analysis}} + \delta^2_{\text{sample range}} + \delta^2_{\text{bioturbation}}\right)}$$

[26] Before calibration we also need to allow for the additional 2 SE uncertainty in the correlation framework.

$$\delta_{\text{total}} = \sqrt{\left(\delta^2_{\text{sampling uncertainty}} + \delta^2_{\text{correlation}}\right)}$$

Calibration will propagate and increase these errors. Even in LC-21 (no correlation error) the median datings from calibration have an average $2\sigma$ range of 1710 years or ±855 years and a high of 2822 (±1411 years). This is similar to the error size suggested by the uncalibrated ages by *Jorissen et al.* [1993]. This suggests these age differences are real and that individual datings may be rather misleading. Fortunately we can substantially reduce these errors by constructing a time framework model that benefits from error reduction by multiple datings.

## 7. Marine Reservoir Effect

[27] Before calibrating we must also assess the size of the marine reservoir effect. Foraminifera fix carbon (including $^{14}C$) in the form of calcite from carbonate and bicarbonate ions in seawater. $^{14}C$ atoms are formed in the upper atmosphere by the addition of a neutron and loss of a proton from abundant $^{14}N$ (present as molecular nitrogen $N_2$). These $^{14}C$ atoms immediately start to decay back to $^{14}N$ (by emission of a beta particle, $^{0}\beta$). Radioactive $^{14}C$ reacts with oxygen to form $CO_2$ and is incorporated into the atmospheric carbon budget. In the oceans, only surface waters can freely exchange $CO_2$ and hence take up this atmospheric $^{14}C$ signal [*Broecker and Peng*, 1974]. As ocean waters are mixed away from the surface, $^{14}C$ lost by radioactive decay is not longer replaced by exchange with the atmosphere. Hence all marine waters show an aging $^{14}C$ signal and the longer a water mass is removed from the surface exchange the older the radiocarbon signal [*Mangerud*, 1972]. This means that any marine (foraminiferal) calcite will show an older radiocarbon age than its true age, because of the inclusion of this old carbon [*Berger et al.*, 1966]. The amount of old carbon is controlled by the depth/region of the calcite growth, the circulation regime of this site and any life effects involved in the deposition of the calcite [*Mangerud*, 1972]. Clearly, this will vary both spatially and temporally, and a "true" reservoir age is normally impossible to determine. In practice, estimates of this reservoir age are a combination of an averaged whole ocean reservoir age of 405 years plus a local correction termed ΔR. This local correction is based on averages of several measurements across large areas, often over whole ocean basins, with an error value quoted to account for possible spatial variability and accuracy in the measurement process [*Stuiver et al.*, 1986].

[28] In addition, a number of closed system assumptions are normally made: (1) that there is no influx of old carbon into the basin, e.g., from terrestrial/riverine sources; and (2) that the sample material accurately records the age of the horizon in which it is found (i.e., no bioturbation or redeposition).

[29] This can lead to considerable inaccuracies. For example even in the highly laminated (annually) varved sediments of the Cariaco Basin with no bioturbation and little fluvial input, foram ages show a standard deviation from the varved determined age model of 42 $^{14}C$ years [*Hughen et al.*, 2004b]. Hughen et al. also note potential age falsifications due to contamination in some individual samples of up to 145 years.

[30] Within the Mediterranean, *Reimer and McCormac* [2002] suggest that there is statistically no difference between reservoir age results recorded in all of the basins including the Aegean basin. They suggested a local reservoir age correction (ΔR) of 58 ± 85 $^{14}C$ years for the last 6000 years. This ΔR is based on the measurement of four marine shells in the Aegean, a further four from the wider eastern Mediterranean, and 26 measurements in the rest of the Mediterranean Sea. They also suggest that before 6000 years B.P., changes in deep water circulation should be taken into account, notably during the period of sapropel deposition between 6000 and 9000 $^{14}C$ years B.P. that is known to have been characterized by reduced deep water ventilation [*Rohling*, 1994; *Kallel et al.*, 1997; *Mercone et al.*, 2000; *Casford et al.*, 2003]. A single shell determination of ΔR during this period of sapropel deposition gives a ΔR value of 149 ± 30 years [*Facorellis et al.*, 1998]. Before 9000 years B.P., circulation in the Aegean appears to have generally been similar to the modern since ~18,000 years B.P. [*Casford et al.*, 2002]. For ages older than 18,000 $^{14}C$ years B.P., ΔR is harder to model, since lower sea levels reduced the shallow shelf areas essential for deep water production but colder temperatures increased the density of the surface waters. *Siani et al.* [2001] attempted to resolve uncertainty prior to 12,000 years B.P. by dating planktonic foraminifera associated with marine tephras. They determined seven values for surface water age over the last 18,000 years, five of which correspond to the modern values during the Holocene, Younger Dryas and the Last Glacial Maximum. The remaining two values at 15 700 and 17,000 years B.P. both show noticeable increases in surface water age. However, this calculation assumes no bioturbation in the marine samples. Siani et al. explicitly state this assumption, justifying it by pointing to the high sedimentation rate of "~35 cm in 1000 years". This is somewhat problematic, since such marine tephras are normally found as admixtures of marine ooze and ash and do not preclude normal bioturbation processes after deposition. Moreover when such layers comprise pure ash they do not prevent bioturbation until the time of the tephra placement. Thus even low bioturbation rates of the order of 10 cm [*Casford et al.*, 2002] would suggest that inaccuracies of the order of 300 years remain possible. Still the arguments of *Siani et al.* [2001] for older surface waters in this period are both

interesting and persuasive. Siani et al. also state that they cannot rule out the possibility that the two datings showing water ages older than expected, are short-lived events and constrain these excursions in $\Delta R$ to the year ranges [*Siani et al.*, 2001]. As the dates used here do not fall in either of these excursions and the bioturbation argument is not comprehensively addressed by *Siani et al.* [2001] we use a value for $\Delta R$ of 58 ± 85 $^{14}C$ years below the sapropel [*Reimer and McCormac*, 2002]. This is consistent with Siani et al.'s five remaining datings.

## 8. Error Reduction

[31] Multiproxy studies within the radiocarbon dating range are often supported by about 10 AMS $^{14}C$ datings, for reasons of economy and practicality (i.e., availability of material). By using these datings to construct an age model, some error reduction (relative to individual values) can be achieved. This reduction is proportional to $1/\sqrt{n}$ where n is the number of analyses. Thus analyzing 10 samples will reduce the standard error for the framework to 31% of the average error for individual analyses. Thirty datings are required to obtain an error reduction to 18% of the total spread of data and more than 100 samples to reduce this to below 10%. Beyond 30 samples, increasing the number of datings results in only small (and decreasing) improvements in precision. We provide 30 datings inside our correlatable boundaries. This allows us to determine a calibrated age model that benefits from this error reduction. We determine that the calibrated time frame (Figures 5 and 6) provides an age model with uncertainties of the order of ±350 years. Addition of more datings is unlikely to lead to substantial improvements through error reduction.

[32] These considerations dictate that future studies in marine cores using microfossil material require at least 30 datings to constrain the chronology in systems where sediment deposition appears linear. Relating a new core to our framework would offer a cheap and easily applied tool to apply maximal error reduction for the time-stratigraphic framework of new Mediterranean cores. Every additional AMS dating correlated into our framework helps to further improve its accuracy and usefulness. We emphasize that the main effort to improve the framework is best targeted at extending the upper and especially lower boundaries of the correlated interval.

## 9. Conclusions

[33] Material used in individual marine AMS $^{14}C$ datings is normally a composite of both contemporaneous and allochtonous material. This present study quantifies the total statistical error resultant from this composite. AMS dates on planktonic foraminifera or other similar material must account for the recorded variance, with the literature and the $2\sigma$ (95% of variance) results in our study suggesting the uncertainties in individual AMS datings are of the order of 1300 years.

[34] To optimize error reductions in the chronostratigraphic of a single core, at least 30 data points are required. Our method offers a standard eastern Mediterranean framework with 30 datings already in place, and allows optimum error reduction to the time framework of any core correlated into this framework. This framework currently gives error values of ±240 years (2 SE) for our uncalibrated time framework and ±350 years ($2\sigma$, 95% variance) in the calibrated time framework.

[35] Correlation of additional cores to this framework would improve these uncertainties. For correlation to the framework a strict application of the events identified here from records of multiple proxies, is required. These records should in addition rely on proxy measurements taken on same/equivalent depth samples, to ensure similar bioturbation effects etc. for all proxies in the core. The method works best if sampling resolution is better than ~200 years ensuring accurate placement of events and hence dating accuracy.

## References


Bard, E. (2001), Paleoceanographic implications of the difference in deep-sea sediment mixing between large and fine particles, *Paleoceanography*, *16*, 235–239.

Bard, E., M. Arnold, P. Maurice, and J. C. Duplessy (1987), Measurements of bomb radiocarbon in the ocean by means of accelerator mass-spectrometry: Technical aspects, *Nucl. Instrum. Methods Phys. Res., Sect. B*, *29*(1–2), 297–301.

Berger, R., R. E. Taylor, and W. F. Libby (1966), Radiocarbon content of marine shells from California and Mexican west coast, *Science*, *153*(3738), 864–865.

Bethoux, J. P., B. Gentili, P. Morin, E. Nicholas, C. Pierre, and D. Ruiz-Pino (1999), The Mediterranean Sea: A miniature ocean for climatic and environmental studies and a key for climatic functioning of the North Atlantic, *Prog. Oceangr.*, *44*, 131–146.

Broecker, W. S., and T. H. Peng (1974), Gas-exchange rates between air and sea, *Tellus*, *26*, 21–35.

Bromley, R. G., and N. Hanken (2003), Structure and function of large lobed Zoophycos Pliocene of Rhodes, Greece, *Palaeogeogr. Palaeoclimatol. Palaeoecol.*, *192*, 79–100.

Calvert, S. E. (1983), Geochemistry of Pleistocene sapropels and associated sediments from the eastern Mediterranean, *Oceanol. Acta*, *6*, 255–267.

Casford, J. S. L., et al. (2001), Mediterranean climate variability during the Holocene, *Mediter. Mar. Sci.*, *2*(1), 45–56.

Casford, J. S. L., E. J. Rohling, R. Abu-Zied, S. Cooke, C. Fontanier, M. Leng, and V. Lykousis (2002), Circulation changes and nutrient concentrations in the Late Quaternary Aegean Sea: A nonsteady state concept for sapropel formation, *Paleoceanography*, *17*(2), 1024, doi:10.1029/2000PA000601.

Casford, J. S. L., E. J. Rohling, R. H. Abu-Zied, C. Fontanier, F. J. Jorissen, M. J. Leng, G. Schmiedl, and J. Thomson (2003), A dynamic concept for eastern Mediterranean circulation and oxygenation during sapropel formation, *Palaeogeogr. Palaeoclimatol. Palaeoecol.*, *190*, 103–119.

De Rijk, S., E. J. Rohling, and A. Hayes (1999), Onset of climatic deterioration in the eastern Mediterranean around 7 ky BP: Micropalaeontological data from Mediterranean sapropel interruptions, *Mar. Geol.*, *153*, 337–343.

Dickens, G. R. (2001), Sulfate profiles and barium fronts in sediment on the Blake Ridge: Present and past methane fluxes through a large gas hydrate reservoir, *Geochim. Cosmochim. Acta*, *65*, 529–543.

Facorellis, Y., Y. Maniatis, and B. Kromer (1998), Apparent $^{14}C$ ages of marine mollusk shells from a Greek island: Calculation of the marine reservoir effect in the Aegean Sea, *Radiocarbon*, *40*, 963–973.

Fatela, F., and R. Taborda (2002), Confidence limits of species proportions in microfossil assemblages, *Mar. Micropaleontol.*, *45*, 169–174.

Fontugne, M. R., M. Paterne, S. E. Calvert, A. Murat, F. Guichard, and M. Arnold (1989), Adriatic deep water formation during the Holocene; implications for the reoxygenation of the deep Mediterranean Sea, *Paleoceanography*, *4*, 199–206.

Geraga, M., S. St. Tsaila-Monopolis, C. Ioakim, G. Papatheodorou, and G. Ferentinos (2000), Evaluation of palaeoenvironmental changes during the last 18,000 years in the Myrtoon

basin, SW Aegean Sea, *Palaeogeogr. Palaeoclimatol. Palaeoecol.*, *156*, 1–17.

Hayes, A., E. J. Rohling, S. De Rijk, D. Kroon, and W. J. Zachariasse (1999), Mediterranean planktonic foraminifera faunas during the last glacial cycle, *Mar. Geol.*, *153*, 239–252.

Hemleben, C., M. Spindler, and O. R. Anderson (1989), *Modern Planktonic Foraminifera*, 363 pp., Springer, New York.

Higgs, N. C., J. Thomson, T. R. S. Wilson, and I. W. Croudace (1994), Modification and complete removal of eastern Mediterranean sapropels by postdepositional oxidation, *Geology*, *22*, 423–426.

Hughen, K. A., et al. (2004a), Marine04 Marine radiocarbon age calibration, 26–0 ka BP, *Radiocarbon*, *46*, 1059–1086.

Hughen, K. A., J. R. Southon, J. H. B. Chanda, B. Frantz, and P. Zermeñ (2004b), Cariaco basin calibration update: Revisions to calendar and $^{14}$C chronologies for core Pl07-58PC, *Radiocarbon*, *46*, 1161–1187.

Jorissen, F. J., A. Asioli, A. M. Borsetti, L. Capotondi, J. P. de Visser, F. J. Hilgen, E. J. Rohling, K. van der Borg, C. Vergnaud Grazzini, and W. J. Zachariasse (1993), Late Quaternary central Mediterranean biochronology, *Mar. Micropaleontol.*, *21*, 169–189.

Kallel, N., M. Paterne, J. C. Duplessy, C. Vergnaud-Grazzini, C. Pujol, L. Labeyrie, M. Arnold, M. Fontugne, and C. Pierre (1997), Enhanced rainfall in the Mediterranean region during the last sapropel event, *Oceanol. Acta*, *20*, 697–712.

Li, X., B. Coles, M. Ramsey, and I. Thornton (1995), Sequential extraction of soils for multi-element analysis by ICP-AES, *Chem. Geol.*, *124*(1–2), 109–123.

Löwemark, L., and F. Werner (2001), Dating errors in high-resolution stratigraphy: A detailed X-ray radiograph and AMS-$^{14}$C study of *Zoophycos* burrows, *Mar. Geol.*, *177*, 191–198.

Mangerud, J. (1972), Radiocarbon dating of marine shells, including a discussion of apparent age of recent shells from Norway, *Boreas*, *1*, 143–172.

Mercone, D., J. Thomson, I. W. Croudace, G. Siani, M. Paterne, and S. Troelstra (2000), Duration of S1, the most recent sapropel in the eastern Mediterranean Sea, as indicated by accelerated mass spectrometry radiocarbon and geochemical evidence, *Paleoceanography*, *15*, 336–347.

Mercone, D., J. Thomson, R. H. Abu-Zied, I. W. Croudace, and E. J. Rohling (2001), High-resolution geochemical and micropaleontological profiling of the most recent eastern Mediterranean sapropel, *Mar. Geol.*, *177*, 25–44.

Pujol, A., and C. Vergnaud Grazzini (1995), Distribution patterns of live planktic foraminifera as related to regional hydrography and productive systems of the Mediterranean Sea., *Mar. Micropaleontol.*, *25*, 187–217.

Reimer, P. J., and F. G. McCormac (2002), Marine radiocarbon reservoir corrections for the Mediterranean and Aegean Seas, *Radiocarbon*, *44*, 159–166.

Rohling, E. J. (1994), Review and new aspects concerning the formation of Mediterranean sapropels, *Mar. Geol.*, *122*, 1–28.

Rohling, E. J., and W. W. C. Gieske (1989), Late Quaternary changes in Mediterranean Intermediate Water density and formation rate, *Paleoceanography*, *4*, 531–545.

Rohling, E. J., J. F. Jorissen, C. Vergnaud-Grazzini, and W. J. Zachariasse (1993), Northern Levantine and Adriatic Quaternary planktic foraminifera; Reconstruction of paleoenvironmental gradients, *Mar. Micropaleontol.*, *21*, 191–218.

Rohling, E. J., M. Den Dulk, C. Pujol, and C. Vergnaud-Grazzini (1995), Abrupt hydrographic change in the Alboran Sea (western Mediterranean) around 8000 yrs BP, *Deep Sea Res.*, *42*, 1609–1619.

Rohling, E. J., F. J. Jorissen, and H. C. De Stigter (1997), 200 year interruption of Holocene sapropel formation in the Adriatic Sea, *J. Micropaleontol.*, *16*, 97–108.

Rohling, E. J., P. A. Mayewski, R. H. Abu-Zied, J. S. L. Casford, and A. Hayes (2002), Holocene atmosphere-ocean interactions: Records from Greenland and the Aegean Sea, *Clim. Dyn.*, *20*, 257–267.

Rohling, E. J., et al. (2004), Reconstructing past planktic foraminiferal habitats using stable isotope data: A case history for Mediterranean sapropel S5, *Mar. Micropaleontol.*, *50*, 89–123.

Sarnthein, M., et al. (2000), Exploring Late Pleistocene climate variations, *EOS Trans. AGU*, *81*(51), 625–630.

Siani, G., M. E. Paterne, R. Sulpizio, A. Sbrana, M. Arnold, and G. Haddad (2001), Mediterranean Sea surface radiocarbon reservoir age changes since the Last Glacial Maximum, *Science*, *294*, 1917–1920.

Stanley, D. J. (1985), Mud redepositional processes as a major influence on Mediterranean margin-basin sedimentation, in *Geological Evolution of the Mediterranean Basin*, edited by D. J. Stanley and F. -C. Wezel, pp. 377–413, Springer, New York.

Stuiver, M., and P. J. Reimer (1993), Extended $^{14}$C data base and revised CALIB 3.0 $^{14}$C age calibration program, *Radiocarbon.*, *35*, 215–230.

Stuiver, M., G. W. Pearson, and T. Braziunas (1986), Radiocarbon age calibration of marine samples back to 9000 cal yr BP, *Radiocarbon*, *28*, 980–1021.

Stuiver, M., P. J. Riemer, E. Bard, J. W. Beck, G. S. Burr, K. A. Hughen, B. Kromer, G. McCormac, J. Van der Plicht, and M. Spurk (1998), INTCAL98 radiocarbon age calibration, 24,000–0 cal BP, *Radiocarbon*, *40*, 1041–1083.

Thomson, J., N. C. Higgs, T. R. S. Wilson, I. W. Croudace, G. J. De Lange, and P. J. M. Van Santvoort (1995), Redistribution and geochemical behaviour of redox-sensitive elements around S1, the most recent eastern Mediterranean sapropel., *Geochim. Cosmochim. Acta*, *59*, 3487–3501.

Thomson, J., D. Mercone, G. J. de Lange, and P. J. M. van Santvoort (1999), Review of recent advances in the interpretation of eastern Mediterranean sapropel S1 from geochemical evidence, *Mar. Geol.*, *153*, 77–89.

Van Os, B. J. H., J. J. Middelburg, and G. J. de Lange (1991), Possible diagenetic remobilisation of barium in sapropelic sediment from the eastern Mediterranean, *Mar. Geol.*, *100*, 125–136.

Van Os, B. J. H., L. J. Lourens, F. J. Hilgen, G. J. De Lange, and L. Beaufort (1994), The formation of Pliocene sapropels and carbonate cycles in the Mediterranean: Diagenesis, dilution and productivity, *Paleoceanography*, *9*, 601–617.

Zachariasse, W. J., F. J. Jorissen, C. Perissoratis, E. J. Rohling, and V. Tsapralis (1997), Late Quaternary foraminiferal changes and the nature of Sapropel S1 in Skopelos Basin, in *Proceedings 5th Hellenic symposium on Oceanography and Fisheries*, vol. 1, pp. 391-394, Natl. Cent. for Mar. Res., Athens.

R. Abu-Zied, Geology Department, Mansoura University, El-Mansoura, 35516, Egypt.

J. S. L. Casford, Department of Geography, Durham University, Science Site, Durham DH1 3LE, UK.

S. Cooke, Department of Earth and Ocean Sciences, University of Waikato, Hamilton, New Zealand.

C. Fontanier, Laboratoire des Bio-Indicateurs Actuels et fossils, UFR Sciences, 49045 Angers, France.

M. Leng, School of Geography, University of Nottingham, Nottingham, NG7 2RD, UK.

A. Millard, Department of Archaeology, Durham University, Science Site, Durham DH1 3LE, UK.

E. J. Rohling and J. Thomson, National Oceanography Centre, European Way, Southampton, SO14 3ZH, UK.